The three-dimensional structure of porin from *Rhodobacter capsulatus* at 3 Å resolution

M.S. Weiss[1], T. Wacker[2], J. Weckesser[3], W. Welte[2] and G.E. Schulz[1]

[1]*Institut für Organische Chemie und Biochemie and* [2]*Institut für Biophysik und Strahlenbiologie, Albertstr., D-7800 Freiburg i.Br., FRG and* [3]*Institut für Biologie II, Mikrobiologie, Schänzlestr. 1, D-7800 Freiburg i.Br., FRG*

The crystal structure of porin from *Rhodobacter capsulatus* strain 37b4 has been solved at 3.0 Å (1 Å = 0.1 nm) resolution by multiple isomorphous replacement and solvent-flattening. The three pores of the trimer are well defined in the electron density map. Each pore consists of a 16-stranded β-barrel which traverses the membrane as a tube. Near its center the tube is narrowed by chain segments protruding from the inner wall of the barrel that form an eye-let with an irregular cross-section of about 6 Å by 10 Å. The eye-let has an axial length of about 10 Å; it defines the exclusion limit for diffusing particles.

Porin; Membrane protein structure; X-ray structure; *Rhodobacter capsulatus*

1. INTRODUCTION

The outer membrane of Gram-negative bacteria contains porins, that are weakly ion-selective channels for small polar solutes with exclusion limits typically around 600 Da [1,2]. In general, porins form trimers that are quite resistant to detergents and proteases. Spectroscopic data indicate that porins contain predominantly β-sheets [3], in contrast to other integral membrane proteins [4–6]. Two-dimensional porin crystals have been extensively studied by electron microscopic methods [7–12]. Three-dimensional porin crystals suitable for X-ray structure analyses [13–15] and a low resolution structure [16] have been reported. Here, we extend the low resolution study of the porin from *Rhodobacter capsulatus* 37b4 to a medium resolution of 3.0 Å and describe the pore geometry.

2. MATERIALS AND METHODS

Cultivation of *Rhodobacter capsulatus* strain 37b4, protein preparation, crystal growing and crystal properties have been described previously [14]. The porin crystals belong to space group R3 with one monomer in the asymmetric unit and crystal axes a_{hex} = 95.3 Å, c_{hex} = 146.8 Å, X-ray reflection intensities were generally measured on a four-circle diffractometer (Siemens-Nicolet, model P2₁) at room temperature. Since the crystals were handled in a buffer containing 23–25% (w/v) polyethylene glycol (average M_r 600) and 0.6% (w/v) detergent [16], crystal slipping was a permanent problem even with siliconized capillary tubes. Part of the data were collected on an area detector (Siemens-Nicolet, model X100) at the EMBL, Heidelberg (see Table I).

Correspondence address: M.S. Weiss, Institut für Organische Chemie und Biochemie, Albertstr. 21, D-7800 Freiburg i.Br., FRG

For the multiple isomorphous replacement (m.i.r.) analysis we extended the data collection of two previously established heavy atom derivatives from 5.9 Å [16] to 3.0 Å resolution. The low resolution K₂PtCl₄ data set was discarded, two new Pt-derivatives were added. The heavy atom parameters were refined [17], the results are given in Table I. The final map showed that most heavy atom sites are adjacent to well-developed electron density.

Using the 'best' multiple isomorphous replacement phases [17], we calculated an electron density map, which showed the pores well. This map was further processed by solvent-flattening [18] using the program version of Leslie [19]. In order to follow fine detail within the pores, we used a rather small radius of 6 Å for the averaging sphere [18]. The solvent level was iteratively adjusted to 40% (4 refinement cycles), 45% (4 cycles) and 50% (7 cycles, last phase angle change below 0.5°), which is 83% of the real solvent plus detergent content of 60% [16]. Visual checks of all masks showed that they did not cut into density of interest. The procedure caused an average phase angle change of 54° and yielded a mean figure of merit of 0.85.

The resulting phases were used to calculate an electron density map, which was then plotted on perspex as a minimap for chain tracing (scale 1 Å = 2.7 mm). The tracing was checked on a display system (Evans & Sutherland, model PS-330, program FRODO), which was also used to build a poly-alanine model. The amino acid sequence of the analyzed porin is not yet known.

3. RESULTS AND DISCUSSION

The final solvent-flattened m.i.r. map can be subdivided into 3 rather distinct regions: (i) strong well-developed density forming the pore and the trimer interface, (ii) weak globular density regions between the pore trimers, and (iii) very flat solvent. The strong density was interpreted as a polypeptide chain of 276 residues forming the pore, i.e. the tubular 16-stranded β-barrel with chain segments protruding to the inner side. The monomers are well-connected to trimers. In the crystal, the strong density regions of the trimers form good contacts in all three dimensions, giving rise

Table I

Multiple isomorphous replacement[a]

Derivative data set[b]	Resolution (Å)	Completeness of data set (%)	Number of sites	Phasing power F/E[c] in shells			
				24–5.9 Å	5.9–4.0 Å	4.0–3.3 Å	3.3–3.0 Å
cis-Pt	5.9	100	6	2.1	–	–	–
cis-Pt	3.3	100	7	1.9	1.3	0.8	–
cis-Pt[d]	3.0	75	5	0.9	0.8	0.6	0.5
Terpy	3.6	100	7	1.5	0.8	0.4	–
K₂PtI₆	4.0	100	5	2.0	1.2	–	–
PIP	5.9	100	6	1.8	–	–	–
UO₂Ac₂	3.6	100	7	1.7	1.5	1.2	–
UO₂Ac₂[d]	3.0	89	5	1.4	1.6	1.5	1.1

[a] The method of Dickerson et al. [17] was used for the refinement. The mean figure of merit was 0.59. The native data set was collected to 2.9 Å resolution on a 4-circle diffractometer. Out to 3.3 Å resolution, all data were measured at least twice and merged. The resulting internal R_F-factors between symmetry-related reflection [20] were about 5%, 10% and 20% in the resolution ranges around 6 Å, 3.3 Å and 3.0 Å, respectively. The diffractometer data set was merged with an area detector data set measured at the EMBL, Heidelberg. The overall R_F-factor between these sets [20] was 10%

[b] The abbreviated derivatives are: cis-Pt, cis-Pt(NH₃)₂Cl₂; Terpy Pt(terpyridin)Cl₂; PIP, di-μ-iodobis(ethylenediamine)-diplatinumnitrate; UO₂Ac₂, uranylacetate

[c] F/E is the ratio between root mean square heavy atom structure factor amplitude and lack of closure error [17]

[d] Data set measured with an area detector at the EMBL, Heidelberg

to the basic scaffold and to reflections out to 3 Å resolution and better. The weak globular density regions look like polypeptides but do not show any clear secondary structure or any chain trace of appreciable length. Most of this density is placed laterally between the trimers in the virtual membrane plane. As judged from its volume the weak density corresponds to about 10000 Da. Adding the M_r of the strong (30000) and of the weak density regions gives 40000, which is consistent with the M_r of 43000 derived from SDS-gel electrophoresis.

The 16 established sequences [21–34] show that the M_r of porins split into groups: 31000 for the three eukaryotic species [21–23], around 37000 [24–31], around 41000 [32,33] and 47400 [34] for prokaryotes. Combining these sequence data with our structure, one may conclude that the basic rigid pore structure has an M_r around 30000 and that the additional residues are only of secondary importance. Assuming that the analyzed porin has indeed an M_r around 40000, these additional residues from the weak density regions, they wobble and contribute little to the packing. Conceivably, they facilitate crystal growth by preordering the trimers laterally. In natural membranes these additional residues may give rise to the observed lateral ordering with inter-trimer distances around 95 Å [8,9,12].

The final electron density map has only been interpreted in the strong density region. The map quality is illustrated in Fig. 1. For long segments, the chain path is clear. There are quite a number of density forks, however, where only one of the alternatives can be correct. Without a sequence at hand, the well-defined chain segments could not be connected unambiguously. Therefore, we decided for the most simple connecting scheme given in Fig. 2. The basic structure of the pore became clear in spite of these problems.
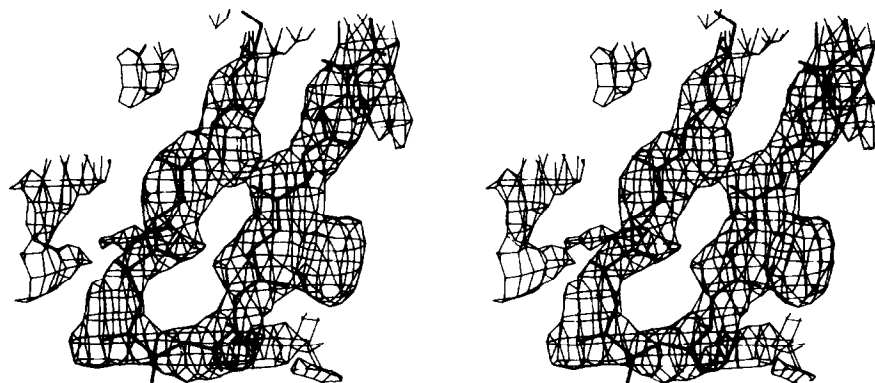

Fig. 1. Quality of the final 3.0 Å solvent-flattened multiple isomorphous replacement electron density map. Depicted are parts of two strands of the 16-stranded β-barrel with their connecting loop built as a poly-alanine model. The sequence is not yet known. The density cut is at 25% of the maximum corresponding to 1.8 standard deviations.
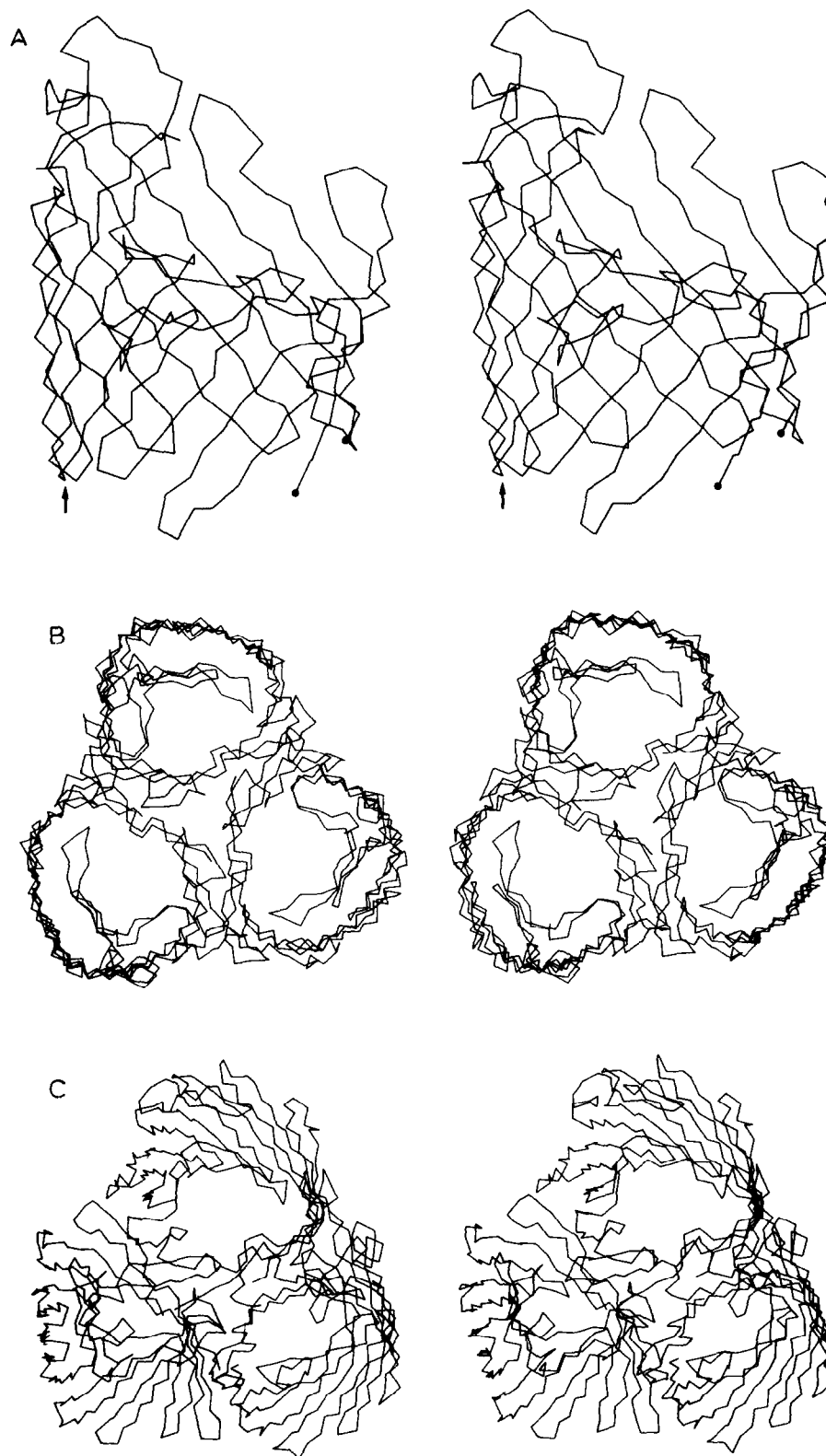
Fig. 2. Stereo drawings of the present C_α-backbone model of porin. (A) Pore monomer consisting of 276 residues that represent the strong density region of the 3.0 Å resolution map. The chain ends are marked by dots and the loop of Fig. 1 by an arrow. The chain outlines the pore well, although not all chain connections are safe so that neither the chain directions nor the β-sheet topology can be considered as final. The chirality is clear from the barrel structure. (B) Pore trimer viewed in a direction close to the 3-fold axis. (C) Pore trimer viewed at an angle of about 35° from the 3-fold axis, showing the intersubunit contacts and the height difference between pore walls at the axis and at the circumference of the trimer in 'triple' (see text).

From the density map it is evident that the monomer pore consists of a 16-stranded β-barrel (Fig. 2A,B). The barrel diameter agrees with electron microscope data [7,10]. The monomer pore can be subdivided into four axially ordered sections which we call 'pipe, cone, eye-let and triple'. The 'pipe' is formed by the barrel wall, it has an elliptic cross-section of about 20×24 Å and an axial length of 8 Å. It is followed by the 'cone' (axial length 8 Å) where the cross-section gradually reduces to its minimum at the 'eye-let'. The 'eye-let' has an irregular cross-section of about 6×10 Å, it extends over an axial length of about 10 Å. It is followed by 'triple' (axial length 14 Å) which, like 'pipe', is defined by the barrel wall. 'Triple' has an elliptical cross-section of 23×27 Å, but in contrast to 'pipe' it lacks one barrel side (at the triad) such that the three pores of a trimer are no longer separated (Fig. 2C).

The map contains no α-helix that could be used as an indicator for determining the map chirality and for assigning the local chain direction. Therefore, the chirality of the map was derived from the β-barrel because only strands proceeding in a right-handed manner with respect to the barrel axis (Fig. 2A) allow for the usual twist of β-sheets [35]. The chain direction remains unsafe. The angles between β-strands and the membrane plane are about 30° near the trimer axis and about 60° at the opposite side of the barrel, which is consistent with the 45° angle derived from spectroscopic data [3]. The smaller angle close to the axis corresponds to the shorter length of the barrel at this side, which forms the trimer interface. The trimer interface contact is very strong, though the present map indicates no chain participation in β-barrels of neighboring subunits. The dissociation of a trimer within the membrane seems unlikely, because the interface contacts are certainly polar as judged from their strong density. At low resolution, it had not been possible to dissect the contacting β-barrels [16].

The present model has a very simple β-sheet topology: all strands are antiparallel and all loops are local. Quite a number of these local loops are safe (Fig. 1), but alternative connections cannot always be excluded. The close proximity of N- and C-termini at the interface has been noticed. The left-hand side of the pore in Fig. 2A has a large protuberance, which to some extent covers the pore (Fig. 2B). It is rigid and forms the most important crystal packing contact. Additional flexible protuberances are likely. It is not yet clear how the weak glubular density regions are connected with the strong density of the pore. Since the weak density is not concentrated in a single region, it is unlikely to form an N- or C-terminal domain.

In conclusion, we present here the shape of the rigid part of the porin trimer in three dimensions. The general paths of the polypeptide segments are clear, the sequence of these segments along the chain may still contain errors. The basic structure is a 16-stranded β-

barrel with tilted strands. Polypeptide chain segments protruding from the barrel wall to the inside define the size of the eye-let and thus the exclusing limit for diffusing particles.

REFERENCES

[1] Nikaido, H. and Vaara, M. (1985) Microbiol. Rev. 49, 1–32.
[2] Benz, R. and Bauer, K. (1988) Eur. J. Biochem. 176, 1–19.
[3] Nabedryk, E., Garavito, R.M. and Breton, J. (1988) Biophys. J. 53, 671–676.
[4] Henderson, R. and Unwin, P.N.T. (1975) Nature 275, 28–32.
[5] Deisenhofer, J., Epp, O., Miki, K., Huber, R. and Michel, H. (1985) Nature 318, 618–624.
[6] Feher, G., Allen, J.P., Okamura, M.Y. and Rees, D.C. (1989) Nature 339, 111–116.
[7] Engel, A., Massalski, A., Schindler, H., Dorset, D.L. and Rosenbusch, J.P. (1985) Nature 317, 643–645.
[8] Chalcroft, J.P., Engelhardt, H. and Baumeister, W. (1987) FEBS Lett 211, 53–58.
[9] Kessel, M., Brennan, M.J., Trus, B.L., Bisher, M.E. and Steven, A.C. (1988) J. Mol. Biol. 203, 275–278.
[10] Jap, B.K. (1989) J. Mol. Biol. 205, 407–419.
[11] Sass, H.J, Büldt, G., Beckmann, E., Zemlin, F., van Heel, M., Zeitler, E., Rosenbusch, J.P., Dorset, D.L. and Massalski, A. (1989) J. Mol. Biol. 209, 171–175.
[12] Rachel, R., Engel, A.M., Huber, R., Stetter, K.-O. and Baumeister, W. (1990) FEBS Lett. 262, 64–68.
[13] Garavito, R.M., Jenkins, J., Jansonius, J.N., Karlsson, R. and Rosenbusch, J.P. (1983) J. Mol. Biol. 164, 313–327.
[14] Nestel, U., Wacker, T., Woitzik, D., Weckesser, J., Kreutz, W. and Welte, W. (1989) FEBS Lett. 242, 405–408.
[15] Stauffer, K.A., Page, M.G.P., Hardmeyer, A., Keller, T.A. and Pauptit, R.A. (1990) J. Mol. Biol. 211, 297–299.
[16] Weiss, M.S., Wacker, T., Nestel, U., Woitzik, D., Weckesser, J., Kreutz, W., Welte, W. and Schulz, G.E. (1989) FEBS Lett. 256, 143–146.
[17] Dickerson, R.E., Weinzierl, J.E. and Palmer, R.A. (1968) Acta Crystallogr. B24, 997–1003.
[18] Wang, B.-C. (1985) Methods Enzymol. 115, 90–112.
[19] Leslie, A.G.W. (1987) Acta Crystallogr. A43, 134–136.
[20] Thieme, R., Pai, E.F., Schirmer, R.H. and Schulz, G.E. (1981) J. Mol. Biol. 152, 763–782.
[21] Mihara, K. and Sato, R. (1985) EMBO J. 4, 769–774.
[22] Kleene, R., Pfanner, N., Pfaller, R., Link, T.A., Sebald, W., Neupert, W. and Tropschug, M. (1987) EMBO J. 6, 2627–2633.
[23] Kayser, H., Kratzin, H.D., Thinnes, F.P., Götz, H., Schmidt, W.E., Eckart, K. and Hilschmann, N. (1989) Biol. Chem. (Hoppe Seyler) 370, 1265–1278.
[24] Inokuchi, K., Mutoh, N., Matsuyama, S. and Mizushima, S. (1982) Nucleic Acids Res. 10, 6957–6968.
[25] Overbeeke, N., Bergmans, H., van Mansfeld, F. and Lugtenberg, B. (1983) J. Mol. Biol. 163, 513–532.
[26] Mizuno, T., Chou, M.Y. and Inouye, M. (1983) J. Biol. Chem. 258, 6932–6940.
[27] Van der Ley, P., Bekkers, A., van Meersbergen, J. and Tommassen, J. (1987) Eur. J. Biochem. 164, 469–475.
[28] Gotschlich, E.C., Seiff, M.E., Blake, M.S. and Koomey, M. (1987) Proc. Natl. Acad. Sci. USA 84, 8135–8139.
[29] Blasband, A.J., Marcotte, W.R., Jr. and Schnaitman, C.A. (1986) J. Biol. Chem. 261, 12723–12732.

[30] Duchêne, M., Schweizer, A., Lottspeich, F., Krauss, G., Marget, M., Vogel, K., Specht, B.U. and Domdey, H. (1988) J. Bacteriol. 170, 155-162.

[31] Venegas, A., Gómez, I., Zaror, I. and Yudelevich, A. (1988) Nucleic Acids Res. 16, 7721.

[32] Stephens, R.S., Mullenbach, G., Sanchez-Pescador, R. and Agabian, N. (1986) J. Bacteriol. 168, 1277-1282.

[33] Barlow, A.K., Heckels, J.E. and Clarke, I.N. (1989) Mol. Microbiol. 3, 131-139.

[34] Clément, J.M. and Hofnung, M. (1981) Cell 27, 507-514.

[35] Schulz, G.E. and Schirmer, R.H. (1979) Principles of Protein Structure, pp. 75-78, Springer-Verlag, New York.